Runaway generation during disruptions in JET and TEXTOR

M. Lehnen [a,*], S.S. Abdullaev [a], G. Arnoux [e], S.A. Bozhenkov [a], M.W. Jakubowski [c], R. Jaspers [b], V.V. Plyusnin [d], V. Riccardo [e], U. Samm [a], JET EFDA Contributors [1], The TEXTOR Team

[a] Institute of Energy Research – Plasma Physics, Forschungszentrum Jülich GmbH, Association EURATOM-FZJ, Jülich, Germany[2,4]
[b] FOM-Rijnhuizen, Association EURATOM-FOM, PO Box 1207, 3430 BE Nieuwegein, The Netherlands[3,4]
[c] Max-Planck-Institut für Plasmaphysik, IPP-EURATOM Association, Teilinstitut Greifswald, Wendelsteinstr. 1, 17491 Greifswald, Germany
[d] Instituto de Plasmas e Fusão Nuclear/IST, Associacao EURATOM-IST, Av. Rovisco Pais, 1049-001 Lisbon, Portugal
[e] EURATOM/UKAEA Fusion Association, Culham Science Centre, OX14 3DB, UK

ARTICLE INFO

ABSTRACT

Runaway electrons generated during ITER disruptions are of concern for the integrity of the plasma facing components. It is expected that a power of up to 8 GW is exposed to ITER PFCs. We present in this article observations from JET and TEXTOR on the generation of runaways and the heat load deposition. Suppression techniques like massive gas injection and resonant magnetic perturbations are discussed.

© 2009 Elsevier B.V. All rights reserved.

1. Introduction

Disruptions impose severe thermal and mechanical loads on tokamak devices. This contribution focuses on runaway electrons (RE). During the current decay phase of a disruption, runaway electrons can be generated in present day devices with energies of some 10's of MeV. Such a runaway beam can carry up to 60% of the initial plasma current [1]. Eventually, this beam is lost to the first wall and can lead to severe damage. As this contribution will show, disruptions in today's devices do not always lead to runaway generation. The occurrence of runaways depends instead on several parameters. However, due to the strong avalanche multiplication, in ITER runaway generation is expected in every disruption [2,3]. Understanding runaway generation and developing suppression mechanisms is thus very important to avoid hazards in ITER disruptions.

In this work, we present results from JET and TEXTOR disruptions. The JET results are based on a systematic analysis of 1628 disruptions. The probability for runaway generation in these disruptions depends on such parameters as the strength of the toroidal magnetic field and the electric field during the current quench. The link between high electric fields and impurity release caused by heavy wall loading during the thermal quench is demonstrated. Complementary results from TEXTOR disruptions, initiated by

massive gas injection of noble gases, will also be presented. Runaway electrons can be generated deliberately by injection of about 10^{22} Argon atoms and a systematic study of their suppression by gas injection as well as their loss mechanisms has been performed. Runaway suppression can also be achieved by increasing losses using resonant magnetic perturbations (RMP). The influence of $n = 1$ and $n = 2$ perturbation fields excited by the helical coils of the dynamic ergodic divertor (DED) on runaway loss has been studied.

2. Runaway electron generation

The generation of runaways was studied, by a systematic survey of JET disruptions from pulse JPN50000 (May 2000) to JPN69626 (January 2007). About 8% of the pulses were terminated by a disruption. For the detection of the runaways the neutron rate is used. An increase of the neutron rate during the current quench was taken as indicator. In this way, runaway electrons with energies exceeding about 10 MeV are detected. In 16% of the cases, no neutron signal was available, and these pulses are not taken into account in the analysis. Runaway electrons were detected in limiter and divertor configurations. In limiter plasmas 43% of the disruptions generate RE, in divertor configuration these are 16%. However, a large fraction of the limiter disruptions were deliberately initiated by impurity gas puffing [4] to provoke runaway generation.

It is assumed, that significant runaway generation takes place in present day devices, when the ratio of toroidal electric field to Dreicer field is larger than 0.01–0.02 [5]. These runaways are the primary population, which can be multiplied by the avalanche pro-

cess [6]. However, the loss by, for example, magnetic fluctuations can prevent from a significant runaway current. Because of the various factors determining the runaway generation, we have chosen in the following to present the probability for runaway generation as function of the main parameters, like e.g. electric and magnetic field.

The maximum electric field during the current quench is deduced from the maximum current decay rate $E = L_P dI_P/dt$, where the inductance L_P is $1.2\mu_0 R_0 l_i/2$ with l_i being the internal inductance as given by EFIT reconstruction before the energy quench. The inductance has been corrected by a factor resulting from the current profile flattening after the thermal quench: $3 - 2\Delta I_P^{max}/I_P$, with I_P^{max} being the maximum current of the current spike occurring after the thermal quench [7]. The probability for runaway generation is given in Fig. 1(a) as a function of the maximum electric field during the current quench. A strong increase of the RE probability is found with increasing electric field. The maximum electric field in this database is about 50 V/m.

As reported earlier from JET [4,8], runaway generation occurs only above a threshold for the toroidal magnetic field of about 2 T (Fig. 1(b)). This threshold is also reported from Tore Supra [9], JT-60U [10] and TEXTOR (see below) and is thus independent from machine size. Moreover, the runaway probability increases significantly for magnetic fields beyond 3 T with a tendency to higher runaway currents [1].

The development of a runaway beam depends strongly on the stability of the plasma column. Plasmas which are strongly vertical unstable and soon lost to the wall do not build up a significant runaway current. This is seen from Fig. 1(c), where the RE generation probability is plotted versus the vertical displacement at the time of the maximum electric field. The displacement is given relative to the value before the disruption. Only smaller displacements can be tolerated for runaway generation and a slightly upward moving plasma is more prone to have runaways.

The degree of conversion of thermal current to runaway current is given in Fig. 2. It increases at high electric fields up to 50% for this database. However, for the data shown here, the electric field increases with plasma current (see discussion below) and discrimination is not possible. Indeed, the conversion efficiency increases also with plasma current. More uncertainties arise if the plasma is lost to the wall before the conversion is finished, which is generally the case for JET disruptions in divertor configuration. Attempts have been made in the past to deduce the strength of the avalanche by modelling the current conversion. However, as mentioned already in [8], because of the exponential dependence of the Dreicer generation rate on parameters which are not precisely known in the current quench, like the electron density, a quantification of
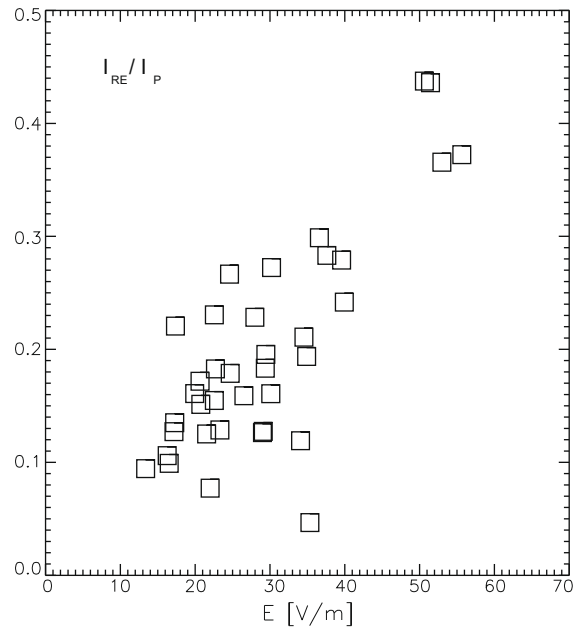

Fig. 2. Runaway conversion efficiency I_{RE}/I_P. The runaway current has been calculated by subtracting an exponential current decay from the measured I_P. Only divertor configuration.

the avalanche in disruptions is difficult. More insight might be gained by measuring the energy spectrum of the runaways.

Fig. 3 gives the parameter space in terms of toroidal magnetic and electric field for JET disruptions. The red dots indicate disruptions with runaway generation. The electric field needed for runaway generation (green dashed curve), increases with decreasing magnetic field, or decreasing safety factor (black lines); a differentiation is not possible. These results are consistent with an earlier analysis, which showed that the maximum q_{95} with runaway generation increases with B_t and that the lower $B_t = 2$ T limit coincides with $q_{95} = 2$ [8].

The minimum magnetic field for runaway generation in TEXTOR is indicated by the blue dots in Fig. 3. These data points result from massive gas injection experiments using Argon (see Section 5). By changing the plasma current from 250 kA to 350 kA, the electric field increases from 13 V/m to 25 V/m. In contrast to the JET observations, the threshold of $B_t \approx 2$ T is independent from E. The safety factor varies from $q_a = 5.5$ to 3.7.
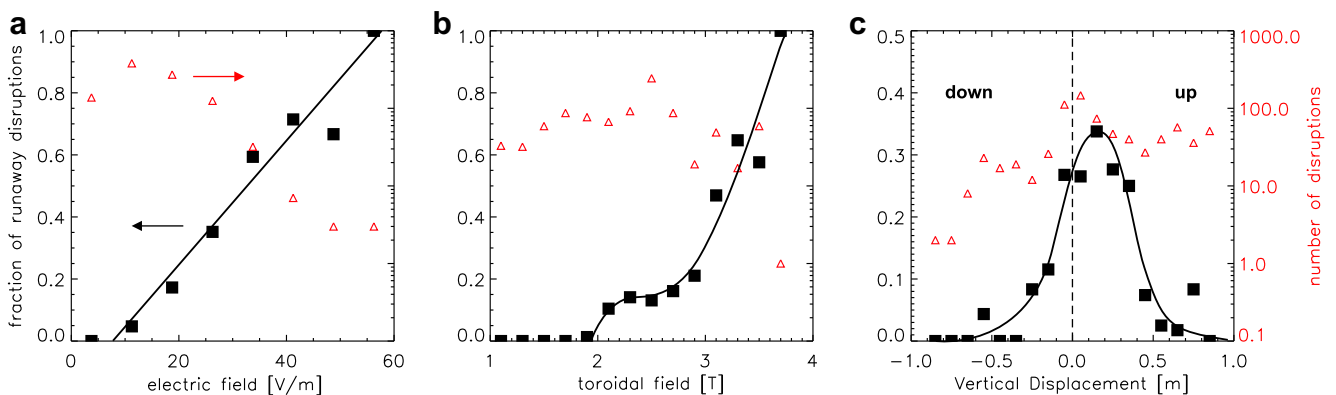

Fig. 1. Probability for the generation of runaway electrons in JET disruptions (JPN50000-69626) as function of: (a) the toroidal maximum electric field during the current quench, (b) the toroidal magnetic field, (c) the vertical displacement at the time of the maximum electric field. Only divertor configurations are considered.
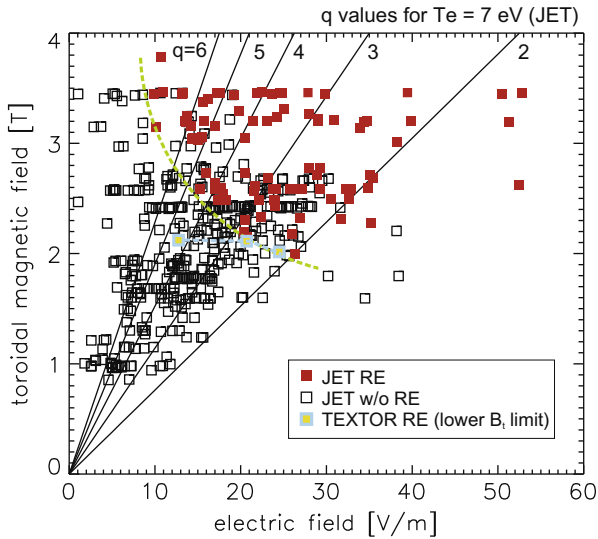
Fig. 3. Parameter space for JET disruptions. The green line indicates the threshold for runaway generation. The boundary for runaway generation in TEXTOR is indicates by the blue line. The safety factor has been estimated from $q_a \approx 2A_P B_t / R_0 \mu_0 I_P$ with $I_P = EA_P / \eta$. (For interpretation of the references to color in this figure legend, the reader is referred to the web version of this article.)
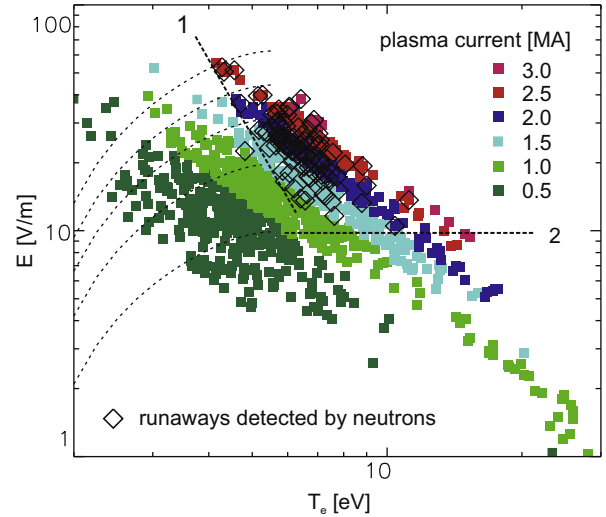

Fig. 4. Toroidal electric field as function of the electron temperature T_e during the current quench. The data is sorted by the plasma current with $\Delta I_P = \pm 0.25$ MA. The electric field depends via the power balance on the carbon density: $E \sim (n_c n_e L_c(T_e))^{1/2} T_e^{-3/4}$. This dependence is indicated by the dashed lines for $n_e = 4 \times 10^{19}$ m^{-3} and $n_c = 0.05, 0.2, 0.5, 1.0, 2.0 \times 10^{19}$ m^{-3}. The limit '1' results from the critical E/E_D ratio to generate a minimum of 100 kA of runaway current. The limit '2' is empiric and extracted from Fig. 3.

3. Electric field

The electric field plays an important role as long as Dreicer generation dominates. This is evident from the exponential increase of the generation rate with E. However, in ITER it is expected that the primary population can also be caused by radiation and thus, the final runaway current would depend only on the initial plasma current, which determines the avalanche multiplication. But especially if loss mechanisms are considered to play a role, the avalanche rate, which is proportional to E, becomes important. This is especially true, if external perturbations are discussed for runaway suppression (see Section 5).

The electric field is a function of the electron temperature and the plasma current according to Ohm's law: $E \sim I_P T_e^{-3/2}$. The temperature has been deduced from the current decay: $T_e = 9.2 \times 10^{-3}$ eV $\cdot (I_P / A_P L_P \dot{I}_P)^{2/3}$, with A_P being the plasma cross-section area and the assumption $Z_{eff} = 1.0$. For the temperatures under discussion, the average charge of the carbon ions is below 4. Depending on the carbon concentration, which we assume to be below 10%, the temperatures might be underestimated by up to 50%.

The electric field as function of the temperature and sorted by the plasma current at the time of the maximum electric field is given in Fig. 4. The temperature ranges between $T_e = 2$ and 20 eV. As expected, T_e increases with higher plasma currents at fixed electric field. At constant I_P, the electric field is increasing with impurity concentration, here carbon density. The carbon density, indicated by the dotted lines, is calculated from corona equilibrium [11] assuming $P_{rad} = P_{OH}$, with $P_{rad} \sim n_e n_C L_C(T_e)$ and $P_{OH} \sim E^2/\eta$. Above the maximum emissivity of carbon at around 6 eV, the corona model might not be applicable in this context and/or radial transport has to be taken into account instead of the 0-D assumption $P_{rad} = P_{OH}$. The impurity release depends on the energy lost during the disruption. This is indicated by an increasing carbon deposition [12] and particle release [13] at higher thermal energies. The disruptions with runaways detected by neutron production are indicated by the black diamonds in Fig. 4. The runaway generation depends not only on the electric field alone, but on the ratio E/E_D. E_D is the so-called Dreicer field, which is proportional to

n_e / T_e [14]. The critical E/E_D to generate at least 100 kA of runaway current is indicated in Fig. 4. Note that $E/E_D \sim I_P / n_e T_e^{0.5}$. To achieve temperatures below this limit, the impurity density and thus the electron density has to be too high to allow for detectable runaway generation (see also discussion in [15]). The limit '2' is an empirical limit taken from Fig. 3 for high magnetic fields. It might be related to the compensation of runaway generation by loss mechanisms or to a decreasing E/E_D at higher temperatures, where $n_e T_e^{0.5}$ could increase again.

4. Runaway dynamics and wall interaction

The limits for the energy impact during transients can be deduced from the one-dimensional solution of the heat diffusion equation in a semi-infinite solid [16]. These limits are defined by the melting/sublimation temperature of the PFC material and are 15 MW m^{-2} s$^{0.5}$ for beryllium and about 40–60 MW m^{-2} s$^{0.5}$ for graphite and tungsten. These estimates are valid, if the heat is deposited at the surface of the PFC. However, because of the high energies in the MeV range, the runaways have a non-negligible penetration depth. Assuming an exponential radial decay of the energy deposition, an analytical formula for the temperature increase can be found [17]:

$$\Delta T = \frac{2q}{K\sqrt{\pi}} \sqrt{\kappa \Delta t} + \frac{q\delta}{K} \left(\exp\left(\delta^2 \kappa \Delta t\right) \text{erfc}\left(\delta\sqrt{\kappa \Delta t}\right) - 1 \right), \tag{1}$$

where $\kappa = K/\rho c$, K is the heat conductivity, c the heat capacity, and ρ the density. δ is the radial e-folding length of the heat source and q is the heat flux density. The deposition duration can be estimated from the final decay of the runaway current: $\tau_{loss} = I_{RE}(dI_{RE}/dt)^{-1}$. This value varies between 2 ms and 5 ms for JET runaway disruptions (Fig. 5). The penetration depth in Be and C is 2.5 mm and 2.0 mm, respectively [18]. The penetration in W is 0.15 mm. A mean energy of $E_{av} = 12.5$ MeV is assumed, which is expected after avalanching [6]. Runaways generated by the Dreicer mechanism gain even higher energies and would penetrate deeper. The resulting critical energy densities are: 6 MJ m^{-2} for Be, 3–5 MJ m^{-2} for W, and 11–13 MJ m^{-2} for C. These values are significantly larger
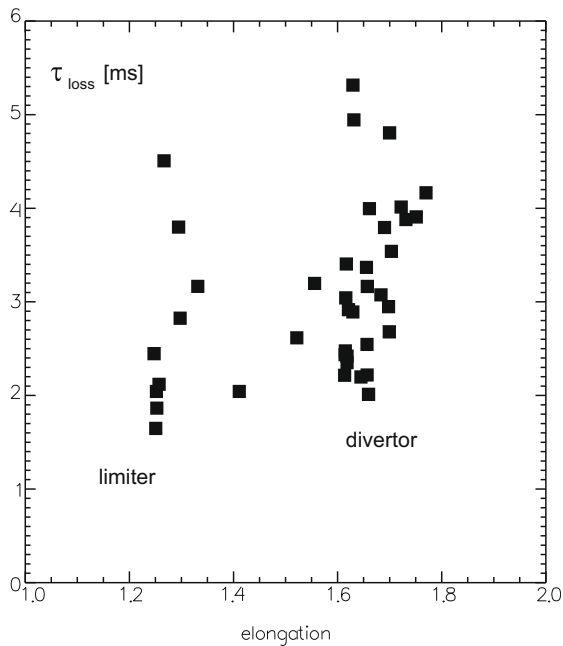
Fig. 5. Decay time of the runaway current for limiter and divertor configuration.
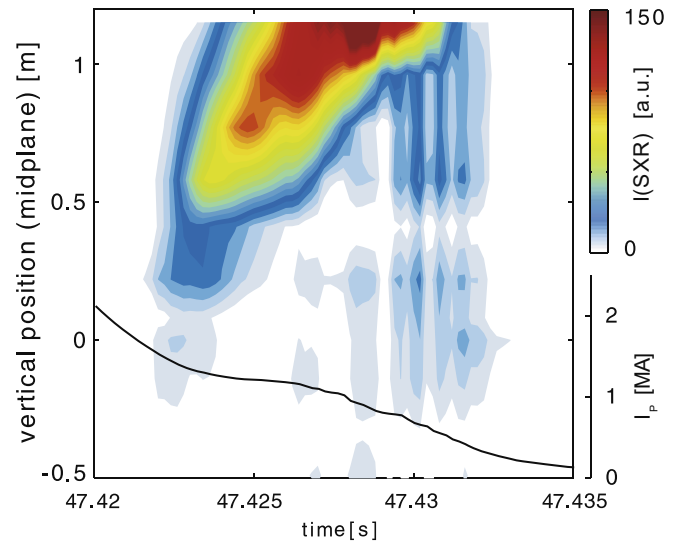

Fig. 6. Soft X-ray radiation during the current quench of JPN 68782. Because of the observation geometry, the vertical position is only indicative.

compared to those for surface deposition: 6–8.5 times for Be, 4.5–6.5 times for C. Because of the shallow penetration, they remain almost unchanged for W. The minimum wetted area needed to prevent from melting/sublimation, $A_{critical}$, is summarised in Table 1. The energies are calculated from $E_{RE} \approx N_{RE}E_{av}$ with $N_{RE} = 2\pi RI_{RE}/ec$. Conversion of magnetic energy as proposed in [2] is not taken into account. The runaway current for the different machines is estimated by assuming a conversion efficiency of 0.6.

For illustration, the heat load generated by runaways will be discussed in the following for the JET pulse 68782. During this disruption a runaway current of 0.48 MA was generated. A runaway plateau of about 5 ms is formed and the runaway beam is finally lost to the upper dump plate. The dynamics of the runaway beam can be detected by the radiation from K-shell vacancy production, which is recorded by the soft X-ray camera [8,19] (Fig. 6). The runaway beam builds up at the vertical center and moves then with a velocity of about 200 m/s upwards while increasing in size. Finally, the beam touches the upper dump plate and releases its energy to the graphite tiles. With a beam radius of about 0.5 m, a heat deposition time of 2.5 ms is estimated. This value is in agreement with the current decay time $\tau_{loss} \approx 3$ ms.

The impact of the runaway beam is detected by the wide-angle IR camera (Fig. 7). Two frames have been recorded during the disruption. The first frame shows a strong temperature increase in the divertor and at the inner poloidal limiter caused by the heat flux during the energy quench. However, on the second frame recorded 20 ms later, a temperature rise at the upper dump plate is visible, which can be attributed to the impact of the runaway beam. This frame is shown in Fig. 7(A). A detail of the upper plate is seen in

Fig. 7(B), giving the temperature difference between the two frames. The maximum temperature rise is about 530 K. The heat is deposited on a very small area of about 0.3 m². The inhomogenous load might result from small misalignments of the tiles, which become significant at shallow angles of incidence.

The heat flux density can be estimated from the above values for runaway current, loss time and runaway energy of 12.5 MeV, to be $q = 400$ MW m^{-2}. The assumption for the energy is supported by the observed neutron production, which has a threshold energy of about 10 MeV. However, the detailed energy spectrum is unknown. According to Eq. (1), this heat load leads to an temperature
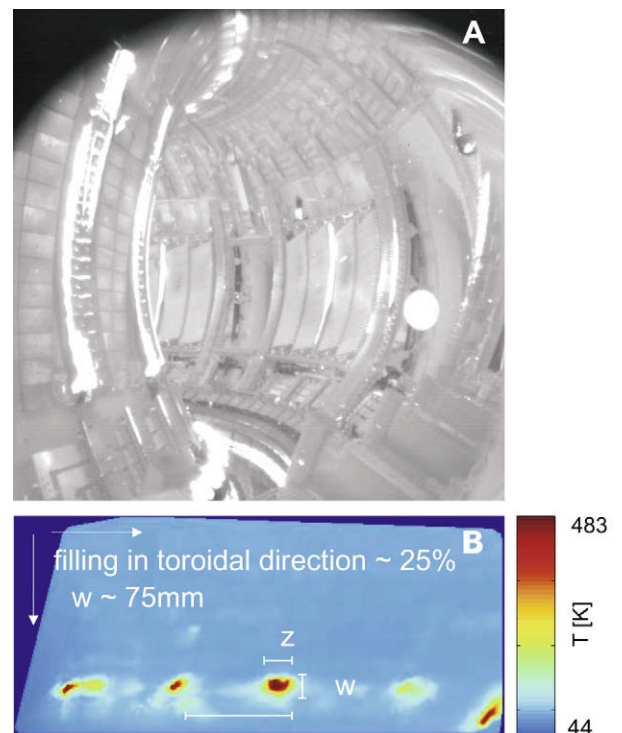
Table 1
Estimated runaway current, total kinetic energy and critical wetted area to prevent from melting/sublimation.

	TEXTOR	JET	ITER
I_{RE} (MA)	0.2	2	9
E_{RE} (MJ)	0.1	1.5	15
$A_{critical}$ (m²)[a]	0.01 (C)	0.25/0.12/0.5	2.5/5/1.4 (Be/W/C)

[a] $\tau_{loss} = 2$ ms.

Fig. 7. Heat load distribution during the disruption of JPN 68782: (A) overexposed overview frame for visualisation, (B) temperature rise at the upper dump plate due to runaway impact.

rise of $\Delta T \approx 330$ K ($\delta = 2$ mm), well in agreement with the measurements. For surface deposition the temperature rise would have been $\Delta T \approx 1500$ K.

5. Runaway suppression

Runaway generation in ITER is dominated by avalanche multiplication. Thus, a mitigation technique has to provide a reliable suppression of this avalanche mechanism. Presently, massive gas injection is discussed as a technique to mitigate forces and heat loads and also to suppress runaway generation [20–26,15]. However, the latter aim might have severe implications which are not easily overcome. Magnetic perturbations by external coils might turn out to be an alternative scheme.

5.1. Massive gas injection

Suppression of runaway generation by massive gas injection requires enormous amounts of gas to be injected into the vacuum vessel. The aim is to increase the critical field for runaway generation $E_c \approx 10^{-21} n_e^\star$ to values, such that $E < E_c$ is fulfilled during the current quench. Here, the density $n_e^\star$ represents bound and free electrons in m^{-3}. The maximum electric field in JET and TEXTOR is about 50 V/m and the same value is assumed for ITER [3]. Thus, a density of $n_e^\star > 5 \times 10^{22}$ m^{-3} has to be achieved for runaway suppression. Here, it has to be kept in mind, that this electric field is a mean value. Radial peaking might make higher densities necessary.

In order to determine the dimensions of the gas injection system for ITER, knowledge about the mixing efficiency is important. The mixing efficiency is defined as the ratio between impurity density in the current quench plasma and the mean density of atoms injected before the energy quench (amount of atoms divided by the vessel volume). The impurity density has been determined by modelling the current quench in TEXTOR disruptions [15]. The mixing efficiency is a function of the gas species (Fig. 8): 3–6% for pure Argon injection, 15–30% for the Argon/Deuterium mixture and above 35–70% for Helium injection. Because of this scaling with impurity mass, the injection of 10^{26} particles into the ITER vessel is required for all three gas species. This results in a neutral pressure in the vessel of 400 Pa and can have serious impact on vacuum systems and machine conditions. However, it has to be clearly stated, that this amount is needed for runaway suppression. The mitigation of forces is already observed for much smaller gas amounts [4,25,26].
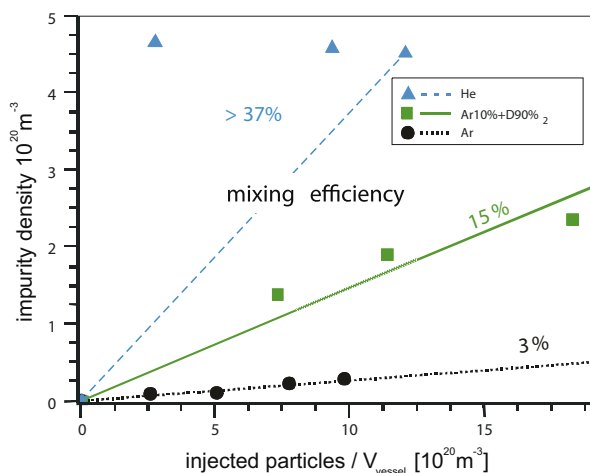
Fig. 8. Massive gas injection at TEXTOR: impurity mixing efficiency during the thermal quench. The mixing efficiency has an error of about +100%.

In present day devices, the required densities for avalanche suppression have not been reached yet. The maximum achieved electron density in TEXTOR using the fast disruption mitigation valve [27] is about $n_e^\star = 8 \times 10^{20}$ m^{-3}. This type of valve has been recently installed at JET and is able to inject up to 6×10^{23} particles. Assuming the same mixing efficiency as in TEXTOR, this will result in an electron density of $n_e^\star = 2 \times 10^{21}$ m^{-3}.

5.2. Resonant magnetic perturbations

Magnetic perturbations cause an enhanced radial loss of RE [28] and could be exploited for runaway suppression. The possibility to suppress runaway generation by using external coils was shown at JT-60 [29]. These experiments have shown that runaways are absent for a sufficiently high perturbation field with base mode number of $m/n = 3/2$. The effect of resonant magnetic perturbations (RMP) on runaway generation has also been studied at TEXTOR during the flat-top phase of low density discharges [30,31]. The perturbation field is produced by the dynamic ergodic divertor (DED) [32]. This divertor consists of 16 helical coils at the high field side of the machine. The base mode numbers of the resulting perturbation field are $m/n = 12/4, 6/2, 3/1$, depending on the chosen connection of the power supplies. Application of a $m/n = 6/2$ perturbation field during the flat-top phase caused a significant decrease of the runaway population above a certain amplitude. This technique has now been applied also to disruptions.

Runaways are deliberately generated by fast injection of 3×10^{21} Argon atoms into an ohmic plasma, with plasma current $I_P = 300$ kA and toroidal magnetic field $B_t = 2.25$ T. This technique generates reliably a runaway current of 100 kA at maximum, with plateaux of up to 50 ms. The DED is energised 200 ms before the gas injection. The current decay rate shows no dependence on the perturbation amplitude and lies between 60 and 80 MA/s. Fig. 9(a) shows the runaway current as function of the perturbation amplitude, represented in coil current normalised to the toroidal mode number. Perturbation fields with $n = 1$ and $n = 2$ were investigated. For $n = 1$ the runaway current is strongly reduced to about 30% of the reference current at coil currents above 1.4 kA/n. Also for $n = 2$ a decrease of I_{RE} can be seen, although with larger scatter. This might be related to the reduced penetration depth of the $n = 2$ field.

Common for both configurations, $n = 1$ and $n = 2$, is the full suppression of high energetic runaways ($W_{RE} > 25$ MeV) above the threshold 1.4 kA/n. This is indicated by the measurements of the synchrotron radiation using the tangential view of a fast IR camera [33]. The maximum of the radial integral from $R = 1.4$ m to 1.9 m is shown in Fig. 9(b). Above the threshold almost all disruptions are free of high energetic runaways. The avalanche process becomes relevant if the runaways can achieve energies above 10–20 MeV [34]. The absence of these, shows that the avalanche is successfully suppressed by RMP, which is consistent with the reduction by a factor 3 in runaway current.

With RMP it is only possible to suppress avalanche generation of runaways. The generation rate for the Dreicer mechanism increases exponentially with electric field and cannot be compensated by RMP induced losses. The enhanced diffusion of thermal particles during RMP is related to a radial field line diffusion, which is described by a field line diffusion coefficient D_{fl} (see for example [35]). High energetic electrons, however, are displaced with respect to the magnetic field line structures. It is therefore necessary to calculate the guiding-center motion of the runaways to quantify the degree of perturbation. The field line diffusion is then replaced by a particle trajectory diffusion D_{pt} [36].

The critical D_{pt} needed to compensate the generation rate can be found from $D_\perp \partial^2 n_{RE}/\partial r^2 = n_{RE}/\tau_{sec}$, with $D_\perp = cD_{pt}$. The runaway generation rate is calculated according to the standard equations,
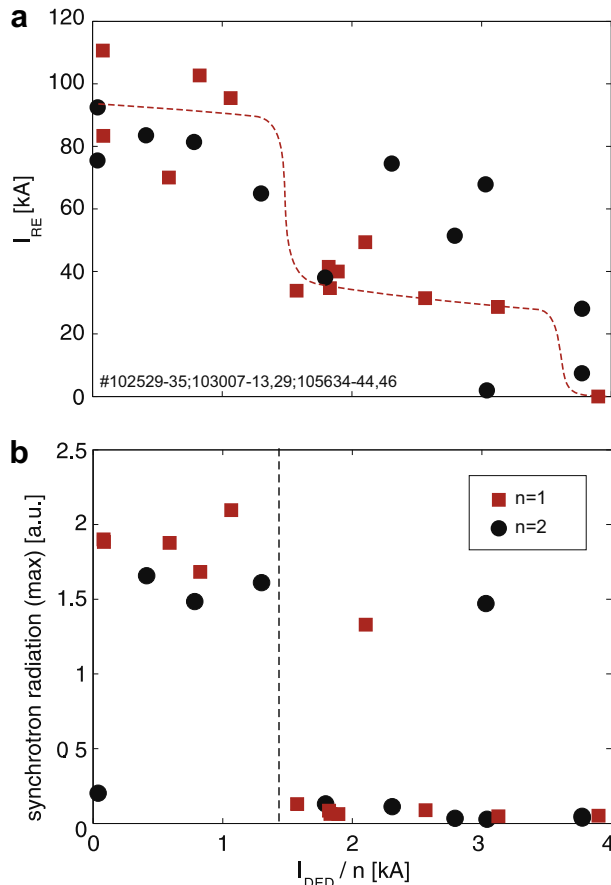
Fig. 9. Runaway suppression by RMP (reproduced from [37]): (a) runaway current as function of the perturbation amplitude, expressed in coil current per toroidal mode number; (b) maximum integral synchrotron radiation as measured by the infra-red camera. Runaways were generated by Argon injection.

which are given for example in [5,15]. For a maximum electric field of $E = 50\,\mathrm{V/m}$ a minimum diffusion coefficient of $D_{pt} = 2 \times 10^{-6}\,\mathrm{m^2/m}$ follows from the above considerations. Calculations for the $n = 1$ experiments using the relativistic formulation of Hamiltonian equations for the guiding-center motion [36], yield values of the order $2-5 \times 10^{-5}\,\mathrm{m^2/m}$ [37]. However, the ergodisation and the related enhanced radial loss depends also on the position of the runaway beam with respect to the perturbation coils. This could also explain the two outliers in Fig. 9.

6. Summary and conclusions

Generation of runaways is seen in 25% of all JET disruptions. The probability for runaway generation increases strongly with increasing toroidal electric field. A lower temperature boundary for runaway generation has been found, which is caused by a strong increase in electron density and therefore an increase in E/E_D for very low temperatures during the current quench. In contrast to ITER, the Dreicer mechanism is the only source for runaways at JET. Extrapolation to ITER would need quantification of the avalanche amplification, which is extremely difficult because of the strong variation of the Dreicer generation rate.

The influence of the toroidal field and/or the safety factor on runaway generation are not fully understood. It might be related to loss mechanisms by magnetic fluctuations, to radial peaking of the electric field, or might indicate a different RE generation process as proposed in [38,39]. We discussed here only the average

electric field, however, closed flux surfaces reestablish during the current quench and current peaking is observed [40]. Dependence of the peaking on toroidal magnetic field is likely and could explain the larger critical average electric field for low B_t (Fig. 3).

Observations of the heat load during runaway disruptions are rare. For the first time, the runaway impact was measured by the wide-angle IR camera at JET. This example shows, that the heat is deposited on an area of about 0.3 m². This area would be already marginally at the melting limit for the ITER-like wall in JET, if runaway currents of 2 MA are generated (cf. Table 1). If the wetted area scales simply with the square of the major radius, a wetted area of 1.5 m² results for ITER. This would marginally prevent from PFC damage in case of C. For Be and W melting is expected. However, the wetted area might increase if perfect alignment and shaping of the ITER PFCs is assumed. Uncertainties exist also for the runaway energy and the angle of incidence. If for example, the energy of the runaways is 50 MeV, significant melting has been reported [41].

The suppression of runaway generation by massive gas injection is challenging, because of the huge amounts of gas to be injected: of the order of 10^{26} particles for ITER, if runaways have to be completely suppressed. Runaway suppression can be established by externally applied magnetic perturbations. The generation of high energetic runaways was suppressed by applying RMP with mode number $n = 1, 2$ in TEXTOR.

Acknowledgements

References

[1] V.V. Plyusnin et al., Nucl. Fus. 46 (2006) 277.
[2] S.V. Putvinski et al., Plasma Phys. Control. Fus. 39 (1997) B157.
[3] T.C. Hender et al., Nucl. Fus. 47 (2007) S128.
[4] V. Riccardo et al., Plasma Phys. Control. Fus. 45 (2003) A269.
[5] P. Helander, L.-G. Eriksson, F. Andersson, Plasma Phys. Control. Fus. 44 (2002) B247.
[6] M.N. Rosenbluth, S.V. Putvinski, Nucl. Fus. 37 (1997) 1355.
[7] R. Yoshino et al., Nucl. Fus. 33 (1993) 1599.
[8] R.D. Gill et al., Nucl. Fus. 42 (2002) 1039.
[9] G. Martin et al., in: 22nd European Physical Society Conference on Plasma Physics and Controlled Fusion, Bournemouth, 1995, II-041.
[10] R. Yoshino et al., Nucl. Fus. 39 (1999) 151.
[11] D.E. Post, J. Nucl. Mater. 220–222 (1995) 143.
[12] A. Kreter et al., J. Nucl. Mater. 390–391 (2009) 38.
[13] V. Philipps et al., J. Nucl. Mater. 390–391 (2009) 478.
[14] H. Dreicer, Phys. Rev. 115 (1959) 238.
[15] S.A. Bozhenkov et al., Plasma Phys. Control. Fus. 50 (2008) 105007.
[16] A. Herrmann, Plasma Phys. Control. Fus. 44 (2002) 883.
[17] H.S. Carslaw, J.C. Jaeger, Conduction of Heat in Solids, Oxford Clarendon, 1959, ISBN 0-19-853368-3.
[18] K. Kanaya, S. Okayama, J. Phys. D: Appl. Phys. 5 (1972) 43.
[19] R.D. Gill et al., Nucl. Fus. 40 (2000) 163.
[20] K.-H. Finken et al., Nucl. Fus. 41 (2001) 1651.
[21] D.G. Whyte et al., Phys. Rev. Lett. 89 (2002) 055001.
[22] G. Martin et al., IAEA, 2004.
[23] M. Bakhtiari et al., Nucl. Fus. 45 (2005) 318.
[24] E.M. Hollmann et al., Nucl. Fus. 45 (2005) 1046.
[25] R.S. Granetz et al., Nucl. Fus. 47 (2007) 1086.
[26] G. Pautasso et al., Nucl. Fus. 47 (2007) 900.
[27] S.A. Bozhenkov et al., Rev. Sci. Instrum. 78 (2007) 033503.
[28] P. Helander, L.-G. Eriksson, F. Andersson, Phys. Plasmas 7 (2000) 4106.
[29] R. Yoshino, S. Tokuda, Nucl. Fus. 40 (2000) 1293.
[30] K.H. Finken et al., Nucl. Fus. 46 (2006) S139.
[31] K.H. Finken et al., Nucl. Fus. 47 (2007) 91.
[32] K.H. Finken et al., Schriften des Forschungszentrum Jülich, Energy Technology, vol. 45, 2005. ISSN 1433-5522.
[33] K.H. Finken et al., Nucl. Fus. 30 (1990) 859.
[34] R. Jayakumar, H.H. Fleischmann, S.J. Zweben, Phys. Lett. A 172 (1993) 447.

[35] S.S. Abdullaev, A. Wingen, K.H. Spatschek, Phys. Plasmas 13 (2006) 042509.
[36] A. Wingen, S.S. Abdullaev, et al., Nucl. Fus. 46 (2006) 941.
[37] M. Lehnen et al., Phys. Rev. Lett. 100 (2008) 255003.
[38] G. Martin, in: 25th EPS Conference on Plasma Physics, Prague, 29 June–3 July 1998, ECA 22C, P-3.006.
[39] H. Smith et al., Phys. Plasmas 12 (2005) 122505.
[40] A. Loarte, ITPA-DSOL Meeting, Avila, 2008.
[41] G. Maddaluno et al., J. Nucl. Mater. 313–316 (2003) 651.